Bistable Helices

Raymond E. Goldstein,[1,2] Alain Goriely,[2,3] Greg Huber,[1] and Charles W. Wolgemuth[1]
[1]*Department of Physics, University of Arizona, Tucson, Arizona 85721*
[2]*Program in Applied Mathematics, University of Arizona, Tucson, Arizona 85721*
[3]*Department of Mathematics, University of Arizona, Tucson, Arizona 85721*
(Received 19 October 1999)

We extend elasticity theory of filaments to encompass systems, such as bacterial flagella, that display competition between two helical structures of opposite chirality. A general, fully intrinsic formulation of the dynamics of bend and twist degrees of freedom is developed using the natural frame of space curves, spanning from the inviscid limit to the viscously overdamped regime applicable to cellular biology. Aspects of front propagation found in flagella are discussed.

PACS numbers: 87.16.–b, 05.45.–a, 46.70.Hg, 47.15.Gf

Over three and a half billion seconds ago, Kirchhoff presented the fundamental equations for elastic rods, the basis for most subsequent theory on the statics and dynamics of elastic filaments [1]. For at least as many *years*, terrestrial life-forms have been engineering and generating all manner of elastic rods, one of the key structural elements of single and multicellular life. It is likely, therefore, that biology has much to teach us about the rich phenomena and inherent possibilities contained within the basic framework of elasticity theory. Here we report one such lesson, namely, the peculiar case of flip-flops of chirality in helical, elastic filaments. The most well-known example of these transitions occurs when the motors that turn helical bacterial flagella reverse direction, causing a coherent bundle of nested flagella to unbundle and the cell body to tumble [2]. Likewise, when such flagella are placed in an external fluid flow, it is observed that regions within the filament periodically flip to the opposite chirality and that those flipped domains propagate steadily downstream [3]. In quiescent fluids, flagella may display two coexisting chiralities (see Fig. 1a). Bacterial fibers [4], chains of bacterial cells formed by repeated cell division without separation, may also display coexistence of two helix hands (Fig. 1b) [5]. Another example is DNA. Recent experiments [6] indicate stretches of left-handed "zigzag" conformation of DNA (Z-DNA) forming spontaneously from right-handed B conformation (B-DNA) due to the stresses generated by twisting during transcription [7].

We present here a simple theory of helical bistability [8], treating it as competition between two states, each locally stable, but of opposite handedness [9]. This differs fundamentally from the phenomenon of *perversion*, seen in vines [10], in which external constraints produce chirality. The bistability of molecular units in bacterial flagella, first advanced by Asakura [11] and later concretely realized as a model by Calladine [12], can be viewed as underlying the continuum approach presented below. Assuming such an underpinning, we extend the energetic formulation of linear elasticity theory by introducing a Landau-Ginzburg functional in the twist strains [13] and, building on earlier work [14–16] develop a fully *intrinsic* formulation of the dynamics applicable to arbitrary twist-energy functionals. Finally, we describe elementary front solutions linking helical states and discuss their biological significance.

The material frame of a filament is an orthonormal triad $\{\hat{\mathbf{e}}_1, \hat{\mathbf{e}}_2, \hat{\mathbf{e}}_3\}$, where we choose $\hat{\mathbf{e}}_3$ along the tangent, $\hat{\mathbf{e}}_1$ pointing toward an imaginary line on the rod surface, and $\hat{\mathbf{e}}_2 = \hat{\mathbf{e}}_3 \times \hat{\mathbf{e}}_1$. The strain vector $\mathbf{\Omega}(s) = (\Omega_1, \Omega_2, \Omega_3)$ characterizes the shape of the filament through the kinematic relation $\partial_s \hat{\mathbf{e}}_i = \mathbf{\Omega} \times \hat{\mathbf{e}}_i$, and the curvature κ satisfies $\kappa^2 = \Omega_1^2 + \Omega_2^2$, with Ω_3 the twist density. We expect the elastic energy $\mathcal{E}[\mathbf{\Omega}]$ to be a Landau expansion, $\mathcal{E} = \sum A_{ij}\Omega_i\Omega_j + \sum B_{ijk}\Omega_i\Omega_j\Omega_k + \cdots$, where symmetry considerations dictate the allowed elastic constants A_{ij}, etc. [13,17]. In *linear* elasticity theory for an isotropic cylindrical rod, the *straight, untwisted* rod minimizes the elastic energy $\mathcal{E} = (1/2)\int ds[A\kappa^2 + C\Omega^2]$, where we adopt the shorthand $\Omega \equiv \Omega_3$. A *helix* is the ground state if the minima of both the curvature and twist energy costs are shifted from zero to *intrinsic curvatures* Ω_1^0, Ω_2^0, and *intrinsic twist* Ω^0. Perhaps the simplest model for a *bistable helix* has an energy with a preferred curvature and *two* stable twist states,

$$\mathcal{E} = \int ds\left[\frac{A}{2}[(\Delta\Omega_1)^2 + (\Delta\Omega_2)^2] + \frac{\gamma^2}{2}\,\Omega_s^2 + V(\Omega)\right], \tag{1}$$

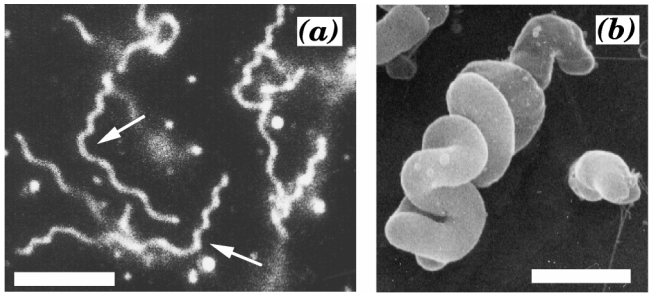

FIG. 1. Bistable helices. (a) Flagella of *Salmonella*, with coexisting left- and right-handed helices (arrows), courtesy of Hotani. (b) Solenoidal form of *B. subtilis* fiber, with coexisting helices, courtesy of Tilby. Scale bars: 5 and 2 μm.

where $\Delta\Omega_i = \Omega_i - \Omega_i^0$, $V(\Omega)$ is a double-well potential and the twist-gradient coefficient γ controls the width of fronts connecting the two states. A most intriguing feature of such fronts is that they correspond to helices concatenated at an angle, as in the examples of Fig. 1.

How do we link such an energy functional to the filament dynamics? The arclength kinematics of the material frame have a complementary temporal kinematics,

$$\partial_t \hat{\mathbf{e}}_i = \boldsymbol{\omega} \times \hat{\mathbf{e}}_i \tag{2}$$

with $\boldsymbol{\omega}$ the rotation rate. It is convenient to trade the material for a "natural" frame $\boldsymbol{\epsilon}$ [16] and use related complex strain and rotation rates,

$$\boldsymbol{\epsilon} = (\hat{\mathbf{e}}_1 + i\hat{\mathbf{e}}_2)e^{i\vartheta}, \tag{3}$$

$$\Psi \equiv \hat{\mathbf{e}}_{3,s} \cdot \boldsymbol{\epsilon} = (-i\Omega_1 + \Omega_2)e^{i\vartheta}, \tag{4}$$

$$\Pi \equiv \hat{\mathbf{e}}_{3,t} \cdot \boldsymbol{\epsilon} = (-i\omega_1 + \omega_2)e^{i\vartheta}, \tag{5}$$

where $\vartheta(s,t) = \int^s ds' \, \Omega$. As they describe the filament shape and velocity, Ψ and Π are related to position and momentum variables in a "Hamiltonian" dynamics (below). [Note that a helix of curvature κ and torsion τ, having then radius $R = \kappa/(\kappa^2 + \tau^2)$ and pitch $p = 2\pi\tau/(\kappa^2 + \tau^2)$, corresponds to $\Psi = \kappa \exp(i\tau s)$.] The kinematics of the natural frame can now be written as

$$\begin{aligned} \partial_s \hat{\mathbf{e}}_3 &= \mathrm{Re}(\Psi \boldsymbol{\epsilon}^*), \qquad & \partial_s \boldsymbol{\epsilon} &= -\Psi \hat{\mathbf{e}}_3 , \\ \partial_t \hat{\mathbf{e}}_3 &= \mathrm{Re}(\Pi \boldsymbol{\epsilon}^*), \qquad & \partial_t \boldsymbol{\epsilon} &= -\Pi \hat{\mathbf{e}}_3 + i(\vartheta_t - \omega)\boldsymbol{\epsilon} , \end{aligned} \tag{6}$$

where we again simplify the notation: $\omega \equiv \omega_3$. The quantities that describe completely the configuration of an elastic filament are now Ψ and Ω, representing the backbone shape and the twist. Using the commutator, $\partial_t \partial_s = \partial_s \partial_t - [\hat{\mathbf{e}}_3 \cdot \mathbf{r}_{t,s}]\partial_s$, with $\mathbf{r}$ the vector of the filament centerline, the kinematic equations become

$$\Omega_t = \omega_s - \Omega \hat{\mathbf{e}}_3 \cdot \mathbf{r}_{t,s} + \mathrm{Im}(\Psi^* \Pi), \tag{7}$$

$$\Psi_t = \Pi_s - \Psi \hat{\mathbf{e}}_3 \cdot \mathbf{r}_{t,s} + \Psi \int^s ds' \, \mathrm{Im}(\Psi^* \Pi). \tag{8}$$

The successive terms in (7) and (8) describe how differential rotation rates cause strain accumulation, the coupling with stretching, and a coupling between twisting and writhing motions. Since $\mathrm{Im}(\Psi^* \Pi) = (\mathbf{r}_s \times \mathbf{r}_{ss}) \cdot \mathbf{r}_{t,s}$, the Ω equation is equivalent to that found in [18]. These purely geometrical relations apply to any moving filament, regardless of the forces that are present.

We close the equations by calculating the force and moment per length acting on the filament. From the principle of virtual work these are functional derivatives of (1); the force per length is $\mathbf{f} = -\delta\mathcal{E}/\delta\mathbf{r}$ with variations in the rotation about the tangent vector, $\delta\chi \equiv \hat{\mathbf{e}}_2 \cdot \delta\hat{\mathbf{e}}_1$, set to zero, while the moment per length about the tangent is $m = -\delta\mathcal{E}/\delta\chi$ with $\delta\mathbf{r} = 0$, giving

$$\begin{aligned} m &= \partial_s\left(\frac{\delta\mathcal{E}}{\delta\Omega}\right) + A \, \mathrm{Im}(\Psi^* \Psi^0), \\ \mathbf{f} &= [\mathrm{Re}(\Phi) - \Lambda_s]\hat{\mathbf{e}}_3 + \mathrm{Re}(\boldsymbol{\epsilon}^* \mathcal{F}_\perp), \end{aligned} \tag{9}$$

with

$$\mathcal{F}_\perp = -A\left[\partial_{ss}(\Psi - \Psi^0) + \frac{1}{2}(|\Psi|^2 - |\Psi^0|^2)\Psi\right] + i\partial_s\left(\frac{\delta\mathcal{E}}{\delta\Omega}\Psi\right) - \Lambda\Psi , \tag{10}$$

where $\Psi^0 = (-i\Omega_1^0 + \Omega_2^0)e^{i\vartheta}$, $\Phi = -A(\Psi - \Psi^0)\partial_s \Psi^{0*}$, and a factor of $\frac{1}{2}\Omega^2$ has been absorbed into the Lagrange multiplier Λ. The second term in the moment equation describes how deformations that are out of the plane of the preferred curvature cause rotation about the tangent.

A dynamical statement is required to close the system. In a normal Newtonian description, forces and moments balance accelerations, $\rho\mathbf{r}_{tt} = \mathbf{f}$ and $m = 2I\omega_t$ with ρ a mass per length, and I is a cross-sectional moment of inertia. The dynamical equations (9) are then the Kirchhoff equations for thin rods with nonlinear constitutive relationships [19]. In the presence of a transverse drag coefficient ζ, an additional force $\zeta\mathbf{r}_t$ appears, while the rotational drag coefficient introduces $m = 2I\omega_t + \zeta_r\omega$. This moment equation closes the twist dynamics; the backbone dynamics are found by taking a spatial derivative and dotting the force equation with $\boldsymbol{\epsilon}$,

$$\rho\left[\partial_t - 2\int^s ds' \, \mathrm{Im}(\Psi^* \Pi) + 2\hat{\mathbf{e}}_3 \cdot \mathbf{r}_{t,s}\right]\Pi + \zeta\Pi = \mathbf{f}_s \cdot \boldsymbol{\epsilon},$$

the equivalent of the momentum equation in a Hamiltonian system. The low Reynolds number regime is attained when the mass density and moment of inertia are zero, forces and moments are balanced by velocities and angular velocities, $\zeta\mathbf{r}_t = \mathbf{f}$ and $m = \zeta_r\omega$, so $\zeta\Pi = \mathbf{f}_s \cdot \boldsymbol{\epsilon}$. Substituting these back into the Ω and Ψ equations, and using linear elasticity theory to define the forces and moments, yields the viscous results found previously [16].

Remarkably, both stationary solutions and moving fronts between bistable states exist for all bistable potentials [8]. Stationary fronts exist when the potential difference ΔV between the twist energy minima (see Fig. 2) vanishes; they connect asymptotically the two stable helical states with opposite torsion and without external mechanical constraints. From (10) we see that the transverse force on the filament vanishes when $\Psi = \Psi^0$ and $\delta\mathcal{E}/\delta\Omega = 0$, namely, when the curvatures have their intrinsic values and Ω is one of its stable states. Then $\Psi^* \Psi^0$ is real and the twisting moment in (9) vanishes. The twist profile satisfies the Euler-Lagrange equation $\gamma^2\Omega_{ss} - V'(\Omega) = 0$. With the Landau model $V = -(r/2)\Omega^2 + (u/4)\Omega^4$, the solution for an infinite filament is $\Omega(s) = \Omega^+ \tanh(s/2\xi)$, where $\Omega^\pm = \pm(r/u)^{1/2}$ and the front width is $\xi = \gamma/(2r)^{1/2}$. In the natural frame, the shape is

$$\Psi = (-i\Omega_1^0 + \Omega_2^0)\exp[2i\xi\Omega^+ \log\cosh(s/2\xi)]. \tag{11}$$

As $s \to \pm\infty$, this solution describes helices with curvature $|\psi|$ and torsion $\Omega^\pm$. To see the real-space relationship between the helices, we go to the limit $\xi \to 0$ and solve the matching problem between one right-handed and one

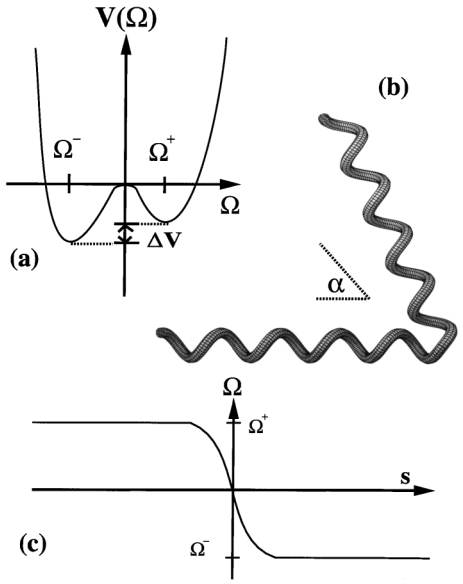

FIG. 2. Description of bistable helices. (a) The double-well potential in the twist variable; (b) a helix corresponding to (c) the elementary front solution of the twist.

left-handed helix. Let the tangents to the right and left helices make angles $\theta_\pm$ with the two (asymptotic) helical axes $z_\pm$. Continuity of the tangents at the junction of the two axes requires that the axes be rotated about the junction by a "block" angle $\alpha = \pi - (\theta_+ - \theta_-)$ (Figs. 2 and 3)

$$\alpha = \tan^{-1}(\tau_+/\kappa_+) - \tan^{-1}(\tau_-/\kappa_-), \qquad (12)$$

where $\kappa_\pm$ and $\tau_\pm$ are the curvature and torsion of the two helices. This simple law, first due to Hotani [20], was intuited through observations of the conformations of reconstituted bacterial flagella. It follows from the geometrical construction in Fig. 3. (Note that θ_- is negative for left-handed helices.) When $\xi \neq 0$, it can be shown that the block angle deviates from (12) through a correction of order $\kappa\tau\xi^2$. Hotani's measurements [20] allow us to estimate [8] an upper bound of $\xi \lesssim 80$ nm.

Consider now solutions propagating between the two minima $\Omega^\pm$ of an asymmetric potential [21]. There are two regimes of interest: inertial and viscous. If, in the former, we deal with potentials V with $\Omega^+ = -\Omega^-$, then a front solution exists propagating along helices of torsion $\Omega^\pm$ (with no external mechanical stress) traveling at a speed $c = \sqrt{|\Delta V|a/2I}$, where ΔV is the potential difference (Fig. 2) and a the cross-sectional area.

In the viscous regime, twist-front motion stems from the overdamped moment-balance relations (7) and (9),

$$\zeta_r \Omega_t = \partial_{ss}\left(\frac{\delta \mathcal{E}}{\delta \Omega}\right) + \cdots, \qquad (13)$$

where the ellipses stand for out-of-plane bending moment variations. Equation (13) is Cahn-Hilliard-like and most reminiscent of model F from the dynamics of critical superfluids [22]. We apply this to the problem of a twist

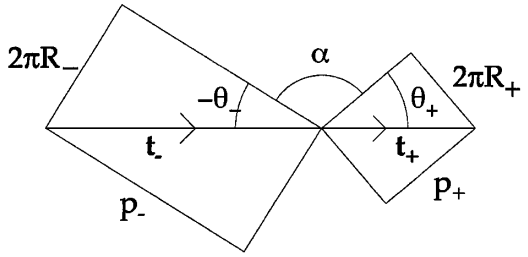

FIG. 3. Geometry for the relation $\theta_+ + \alpha - \theta_- = \pi$. Rectangles are unit cells of the concatenated helices, with radii $R_\pm$, pitches $p_\pm$, and tangents $\mathbf{t}_\pm$.

front moving along a straight rod and propagating between two minima $\Omega^\pm$ of a twist potential $V(\Omega)$ made slightly asymmetric by setting $V(\Omega) = V^{(0)}(\Omega) + \epsilon W(\Omega)$, where $V^{(0)}$ is symmetric, $W = \sum_{n>0} a_n \Omega^n$ is an analytic perturbation, and ϵ controls the degree of asymmetry. The front speed is found by computing the first-order solvability condition (in ϵ) for the existence of a bistable helix in the moving frame $\sigma = s - ct$ [23]:

$$\int \left[\epsilon W'(\Omega^{(0)}) + c\zeta_r \int^\sigma \Omega^{(0)}\, d\sigma'\right]\Omega^{(0)}_\sigma\, d\sigma = 0, \qquad (14)$$

where $\Omega^{(0)}$ is the tanh profile. Hence, the front speed is $c = \epsilon\Gamma\sum_{n\ \mathrm{odd}} a_n(\Omega^+)^{n-2}$, where $\Gamma = 1/\{2\xi\zeta_r[\ln(2) - 1]\}$.

To estimate front velocities involving *helical* shapes (below), note that the essential physics of this result is a balance between the power generated from the transition to the less energetic twist state, $P_{\mathrm{tw}} = (\Delta V)c$, and the power lost due to rotational drag, $P_{\mathrm{rd}} = \int \zeta_r \omega^2 ds = \zeta_r(\Delta\Omega)^2\xi c^2$, where $\omega = (\Delta\Omega)c$ is the axial rotation rate and $\Delta\Omega = \Omega^+ - \Omega^-$, giving $c \sim (\Delta V)/\zeta_r(\Delta\Omega)^2\xi$.

While inertial and viscous front propagation naturally lead to rotation of the unstable helix, there are two types of motion that allow this: *crankshafting*, in which one helix rigidly pivots about the axis of the other, and *speedometer-cable motion* where each helix rotates about its own axis (Fig. 4) [2]. Here we outline simple scaling arguments for these dynamics; a more detailed discussion is presented elsewhere [8]. In a viscous fluid, we might expect the mode requiring the least power dissipation to be favored.

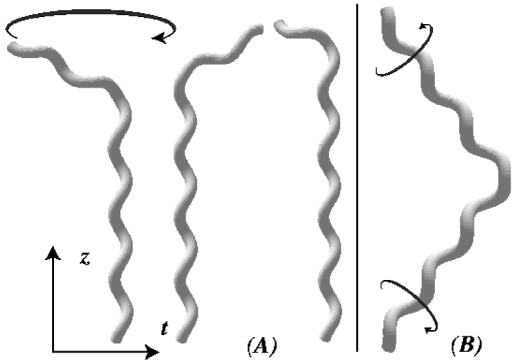

FIG. 4. Front propagation along a helix. Two possible modes are (A) crankshafting and (B) speedometer cabling.

The dissipation P is simply the integrated product of the force per length and the velocity. For crankshafting, $P_{\rm cr} \sim \zeta_\perp \omega^2 L^3 \sin^2(\alpha)/3$, while for speedometer-cable motion $P_{\rm sp} \sim \zeta_\perp R^2 \omega^2 L$, where L is the total arclength of the moving segment. Crankshafting dominates unless $[R/L \sin(\alpha)]^2 \ll 1$, in which case speedometer-cable motion takes over. This argument is similar in spirit to that posed by Levinthal and Crane [24] in the context of DNA transcription. Macnab and Ornston [2] have made dark-field photographs of transitions in *Salmonella* and found evidence for both crankshafting and speedometer-cable motion when R and L were comparable.

Hotani [3] observed that *Salmonella* flagella, fixed at one end in a flow, developed moving fronts of opposite chirality above a certain flow velocity. The fluid flow straightened the flagella, and the fronts propagated by axial rotation, not crankshafting. The torque T_+ estimated to cause the chirality inversion differs from T_-, that to induce the reverse transformation. We estimate the potential difference as $\Delta V \sim T_+\Omega_+ - T_-\Omega_- \sim 1 - 2 \times 10^{-7}$ ergs/cm. Balancing the power generated in converting to the energetically favored state with that lost due to viscous rotation, we find $c \sim \Delta V/[\zeta_\perp R^2(\Delta\Omega)^2 L] \sim 6{-}8\ \mu$m/s, in rough agreement with the observations of $5{-}7\ \mu$m/s. Further, the energy barrier for nucleation of the less-favored chirality state is on the order of $\Delta V_b \xi$, where ΔV_b is the barrier height deduced from those torque estimates. With the previous estimate of ξ we obtain a barrier of 2×10^{-12} ergs, sufficiently greater than thermal energy to prohibit thermally assisted nucleation.

Here we have presented perhaps the simplest continuum theory of bistable helices, illustrating the front solutions corresponding to a set of common scenarios and indicating their relevance for experiments, notably for flagellar systems. A natural extension is to consider such biologically relevant problems as a flagellum cranked at one end by a rotary motor or DNA in the presence of external forces and torques. Our continuum approach connects the phenomenon of bistability at the scale of nanometers [12,25], with the bistability observed at tens of microns [3,26]; it points out, as well, the need for experiments on the rates of chirality transformations under defined conditions of torques and flows, and it provides the possibility for a new level of quantitative description.

We thank D. Coombs, J. O. Kessler, A. I. Pesci, T. R. Powers, C. H. Wiggins, and especially N. H. Mendelson, J. E. Sarlls, and M. Tabor for discussions and ongoing collaborations, and are indebted to M. J. Tilby and H. Hotani for sharing their images. R. E. G. is supported by NSF Grant No. DMR9812526; A. G. is supported by DMS-9972063, NATO-CRG 97/037, and the Sloan Foundation.

[1] G. Kirchhoff, *Vorlesungen uber Mathematische Physik* (B. G. Teubner, Leipzig, 1883).
[2] R. M. Macnab and M. K. Ornston, J. Mol. Biol. **112**, 1 (1977).
[3] H. Hotani, J. Mol. Biol. **156**, 791 (1982).
[4] N. H. Mendelson, Proc. Natl. Acad. Sci. U.S.A. **73**, 1740 (1976).
[5] M. J. Tilby, Nature (London) **266**, 450 (1977).
[6] S. Wölfl, B. Wittig, and A. Rich, Biochim. Biophys. Acta **1264**, 294 (1995); V. Müller *et al.*, Proc. Natl. Acad. Sci. U.S.A. **93**, 780 (1996).
[7] A. Rich and A. Herbert, J. Biol. Chem. **271**, 11 595 (1996); A. Rich, Gene **135**, 99 (1993); A. Wang *et al.*, Science **211**, 171 (1981); see also P. Nelson, Proc. Natl. Acad. Sci. U.S.A. **96**, 14 342 (1999).
[8] Microscopic theories are in A. Goriely *et al.*, University of Arizona report, 1999; D. Coombs *et al.*, University of Arizona report, 1999.
[9] Helices can also arise from symmetry-breaking instabilities where twist does not play a role; see V. Frette *et al.*, Phys. Rev. Lett. **83**, 2465 (1999).
[10] A. Goriely and M. Tabor, Phys. Rev. Lett. **80**, 1564 (1998).
[11] S. Asakura, Adv. Biophys. **1**, 99 (1970).
[12] C. R. Calladine, Nature (London) **255**, 121 (1975); J. Mol. Biol. **118**, 457 (1978).
[13] See J. F. Marko and E. D. Siggia, Macromolecules. **27**, 981 (1994); **29**, 4820 (1996).
[14] K. Nakayama, H. Segur, and M. Wadati, Phys. Rev. Lett. **69**, 2603 (1992); R. E. Goldstein and S. A. Langer, Phys. Rev. Lett. **75**, 1094 (1995).
[15] A. Goriely and M. Tabor, Phys. Rev. Lett. **77**, 3537 (1996); R. D. Kamien, Eur. Phys. J. B **1**, 1 (1998).
[16] R. E. Goldstein, T. R. Powers, and C. H. Wiggins, Phys. Rev. Lett. **80**, 5232 (1998).
[17] Others have proposed nonlinear elastic models based on expansions in powers of κ and the torsion τ [e.g., W. Helfrich, J. Chem. Phys. **85**, 1085 (1986)].
[18] I. Klapper and M. Tabor, J. Phys. A **27**, 4919 (1994); C. W. Wolgemuth, T. R. Powers, and R. E. Goldstein, preceding Letter, Phys. Rev. Lett. **84**, 1627 (2000).
[19] E. H. Dill, Arch. Hist. Exact. Sci. **44**, 2 (1992); A. Goriely and M. Tabor, Physica (Amsterdam) **105D**, 20 (1997); **105D**, 44 (1997).
[20] H. Hotani, J. Mol. Biol. **106**, 151 (1976).
[21] Since the two minima are locally stable there is no velocity-selection problem.
[22] J. W. Cahn and J. E. Hilliard, J. Chem. Phys. **28**, 258 (1958); P. C. Hohenberg and B. I. Halperin, Rev. Mod. Phys. **49**, 435 (1977).
[23] W. van Saarloos and P. C. Hohenberg, Physica (Amsterdam) **56D**, 303 (1992).
[24] C. Levinthal and H. R. Crane, Proc. Natl. Acad. Sci. U.S.A. **42**, 436 (1956).
[25] K. Namba and F. Vonderviszt, Q. Rev. Biophys. **30**, 1 (1997); I. Yamashita *et al.*, Nature Struct. Biol. **5**, 125 (1998).
[26] S. Asakura and T. Iino, J. Mol. Biol. **64**, 251 (1972).